

T3E1 Report: Interference, Entanglement, Quantum-Enhanced Sensing (Quantenkoffer)

6.2410 Quantum Engineering Platforms
Daniel Sanango

I. INTRODUCTION

Throughout this laboratory experience, we explore photon pair generation, observing quantum entanglement, performing single-photon interference measurements, and exploring the Hong-Ou-Mandel (HOM) effect to investigate NOON states. Experiments are done with a Quantenkoffer, a specialized and sensitive machine for the mentioned explorations.

II. DAY 1 APPROACH

The objective of this laboratory exercise was to understand SPDC photon pair generation, alignment, and coincidence measurements, and to use the properties of coincidence detection to measure the speed of light.

To explore these ideas, we were introduced to the Quantenkoffer. The Quantenkoffer features optical and computation tools for single photon generation and quantum entanglement capabilities.

Our first goal was to optimize the counts per second on each APD port (Port A and Port B). Figure 1 demonstrates the optical setup used.

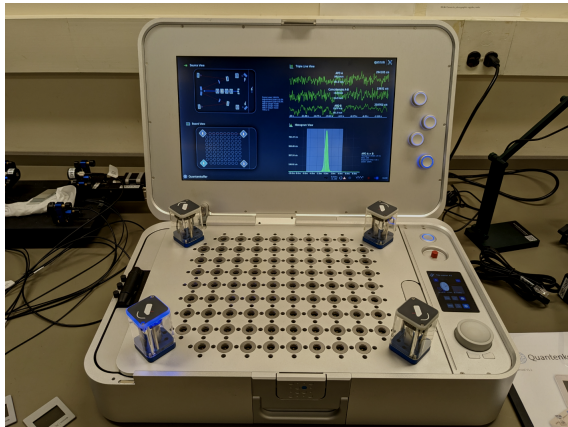


Fig. 1: Setup to Measure Speed of Light [6.2410 Github]

We turned on the Quantenkoffer and placed periscopes on the kit ports. Then, using the Quantenkoffer's UI mirror adjustment tools, we positioned the mirrors on the periscopes to direct photons to the kit's single-photon detectors. To activate the source view, we tapped the top of a source periscope and optimized detector count rates by fine-tuning built-in mirrors.

When adjusting the mirrors, we rotated them very slowly, as even slight changes caused drastic differences in count rates. We took care to note rotations around the x and y axes, adjusting just one axis on both mirrors before moving to the next.

Once we got Port A and Port B's counts above around 100[kcnts/s], we optimized the coincidence counts. We simply re-adjusted the x and y axes of the mirrors, this time caring more about increasing coincidence counts than individual APD counts.

Next, we sought to measure the speed of light using the Quantenkoffer. To do this, we added a beamsplitter and 45 degree mirrors to the system to produce two paths of light propagation. Figure 2 demonstrates the optical setup used.

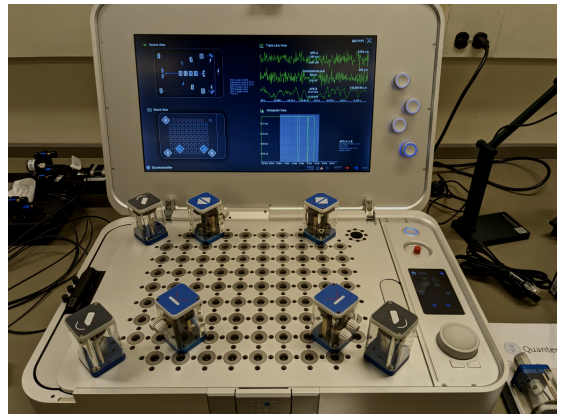


Fig. 2: Setup to Measure Speed of Light [6.2410 Github]

This setup aims to measure the speed of light by determining the time difference between photon arrival times on the Quantenkoffer. By using the propagation path length differences, we would then be able to use $c = \frac{d}{t}$ to estimate the speed of light.

To ensure the different paths were perfectly aligned, we used a low-power adjustment laser to overlap the beam spots in the near-field and far-field. Ensuring both beams overlapped in both fields would ensure a more accurate calculation. Figure 3 demonstrates how we used the Quantenkoffer's monitor area to determine near-field laser alignment. Figure 4 demonstrates a piece of paper far from the beamsplitter to determine far-field laser alignment.

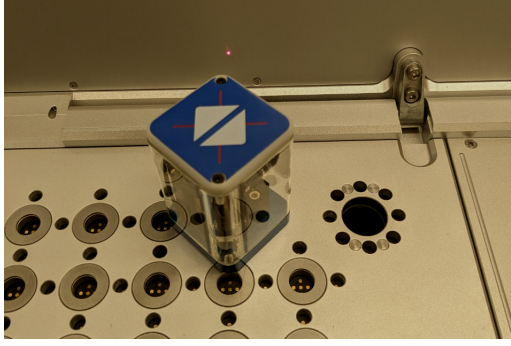


Fig. 3: Near-Field Overlap Calibration Setup [6.2410 Github]

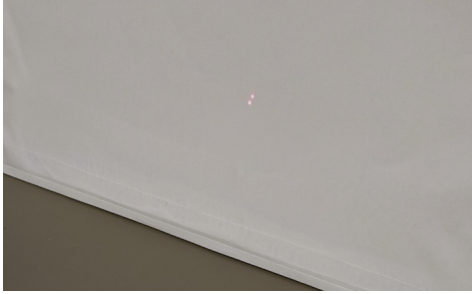


Fig. 4: Far-Field Overlap Calibration Setup [6.2410 Github]

III. DAY 1 RESULTS AND ANALYSIS

After optimizing the coincidence counts, we arrived at these final [cnts/s] values:

Port A: 130[kcnts/s]

Port B: 140[kcnts/s]

Coincidences between A and B: 6[kcnts/s]

Bandwidth: 2.61[ns]

The ratio of coincidences to the average counts per second on ports A and B was $\frac{6 \cdot 10^3}{135 \cdot 10^3} = 0.044$, exemplifying the massive difference between both parameters. A potential explanation for this difference is technical limitations with photon detection methods. While our detectors were able to make picosecond (10^{-12} seconds) bin widths for detection windows, these windows could theoretically be smaller. For instance, femtosecond or attosecond windows would allow for higher coincidence rates, as the photon detectors would be able to sample photon events quicker and, thus, more precisely. Small losses throughout the system such as mirror unidealities and slight misalignments also affect our maximum coincidence statistic. Finally, fiber coupling absorbs a significant amount of photons, blocking a good amount of photons from ever reaching the photon detectors.

Concerning our speed of light measurement, after finalizing our optical setup, we found a peak-to-peak difference of 1.405[ns]. This was quite distinguishable from the Quantenkoffer histogram UI. After this, we determined the path length difference between our paths by measuring a distance between slots on the Quantenkoffer and multiplying by the

number of slots between each optical component. Doing this, we got a path length difference of 43[cm]. Thus, using $c = \frac{d}{t}$...

$$c = \frac{d}{t} = \frac{43[\text{cm}]}{1.405[\text{ns}]} = 298,932,384[\text{m/s}] \quad (1)$$

This is approximately the value for the speed of light.

IV. DAY 2 APPROACH

We started this laboratory exercise by calibrating the coincidence counts as from Day 1. After this, we put a polarizer block in each path. Turning on the continuous rotation on Port B's polarizer, we observed a polar plot of the coincidence counts. We then set the input light polarizations to vertical $|V\rangle$ and horizontal $|H\rangle$, as well as various intermediate angles. Finally, we used quarter waveplates and half waveplates to vary the input polarizations.

V. DAY 2 RESULTS AND ANALYSIS

The shape of the observed polar plots looks like a figure-8. The figure-8 represents the expected sinusoidal probability relation of an entangled pair of photons based on the following math:

$$|\theta_a\rangle = \cos(\theta_a)|H\rangle_a + \sin(\theta_a)|V\rangle_a \quad (2)$$

Thus,...

$$P_{co} = \frac{1}{2} |\langle \theta_b | \{ |H\rangle_a |H\rangle_b + |V\rangle_a |V\rangle_b \}|^2 \quad (3)$$

Expanding this term,...

$$\frac{1}{2} |\cos(\theta_b)\cos(\theta_a) + \sin(\theta_b)\sin(\theta_a)|^2 = \frac{1}{2} \cos^2(\theta_a - \theta_b) \quad (4)$$

Keeping one of the polarization angles constant (in this case, Port A's polarizer) and varying the angle of Port B's polarizer at a uniform angular rate, we find that we expect a polar plot of a figure 8. This is demonstrated in Figure 6, Figure 7, and Figure 5. This demonstrates entanglement because it implies the photon states have a dependence on each other. For instance, if the polarizations of both waves are such that their angles come out to some odd integer multiple of $\frac{\pi}{2}$, we will observe nothing. However, if their angles come out to some integer multiple of pi, we get a maximum output.

When you rotate A manually, we observe a sinusoidal pattern on APD A's c/s, which is expected since this is essentially the same as keeping A static and allowing B to continuously rotate.

When we observe APD B's polar plot, we see a circular pattern. This is because, measuring APD B individually, we observe a circularly-polarized wave (we are measuring the $|+\rangle$ state. Thus, at any angle, we expect to see an equal magnitude of wave intensity, giving the pattern an appearance of $r = \text{constant}$.

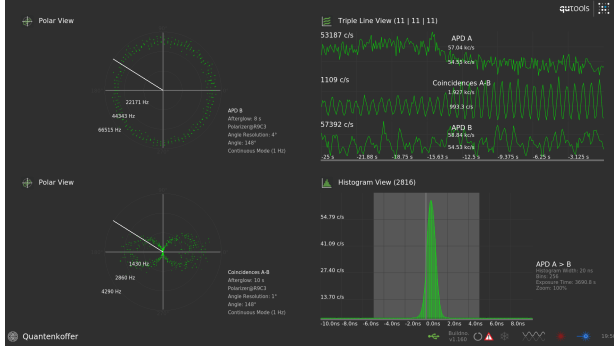


Fig. 5: Source State in $|+\rangle$, A in $|H\rangle$

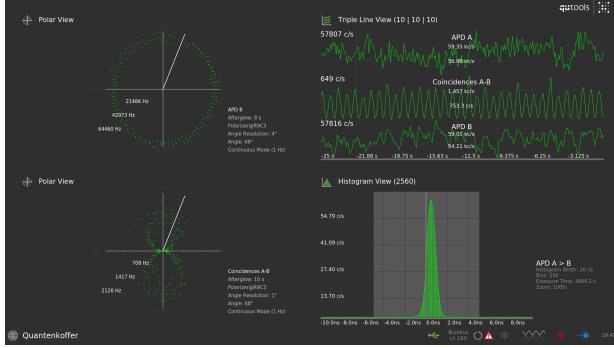


Fig. 6: Source State in $|+\rangle$, A in $|V\rangle$

Next, we put the source in the $|H\rangle$ state and observe the previously-analyzed outputs (result in Figure 8). We once again observe the figure-8 pattern as expected from our calculation, but now APD B's polar plot also looks like a figure-8. This is because the source is in the $|H\rangle$ state, meaning we expect to see no intensity at $\theta = \pm \frac{\pi}{2}$.

Forcing the source polarization in the $|V\rangle$ state and observing the previously-analyzed output (result in Figure 9, the figure-8's are present. We find that, now, at $\theta = \pm \frac{\pi}{2}$, we have peaks instead of nulls. This is because we are in the $|V\rangle$ state, so maximum intensity is expected at these angles.

We now analyze what occurs when a half waveplate is placed before the polarizer on each propagation path.

First, we note the state of B after passing through the half

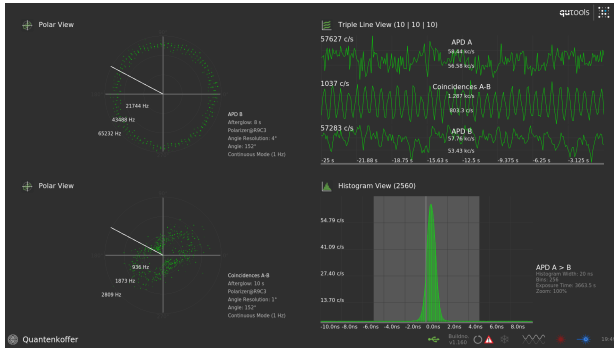


Fig. 7: Source State in $|+\rangle$, A in $|+\rangle$

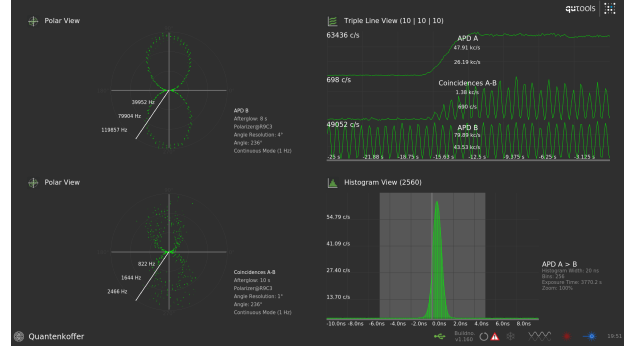


Fig. 8: Source $|V\rangle$, A $|+\rangle$

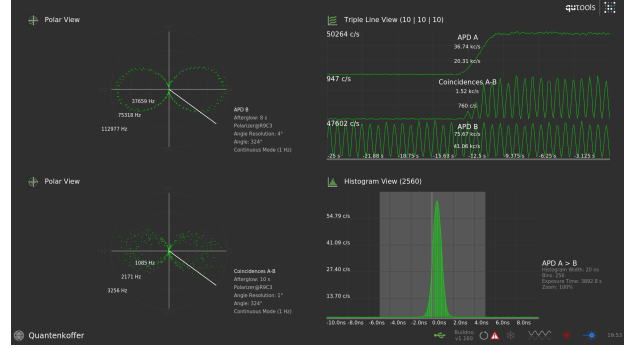


Fig. 9: Source in $|H\rangle$, A in $|+\rangle$

waveplate:

$$|\psi_b\rangle = \frac{1}{\sqrt{2}}(|H\rangle + |V\rangle) \quad (5)$$

States admitted by polarizer:

$$|\theta_b\rangle = \cos \theta_b |H\rangle + \sin \theta_b |V\rangle \quad (6)$$

Measuring the probability of a single count:

$$|\langle \psi_b | \theta_b \rangle|^2 = \left| \frac{1}{\sqrt{2}}(\cos \theta_b + \sin \theta_b) \right|^2 = \frac{1}{2}(1 + \sin(2\theta_b)) \quad (7)$$

This matches our observation from Figure 10. Notably, however, this no longer exhibits entanglement properties, as because of the addition of the waveplate, the polarization states are factorizable. This removes the polarization dependencies entanglement demonstrates.

If we were to use quarter waveplates instead of half waveplates, mathmetically, we would get different results. Analyzing the probability associated with Port B:

$$|\psi_b\rangle = \frac{1}{\sqrt{2}}(j|H\rangle + |V\rangle) \quad (8)$$

Thus,...

$$|\langle \theta_b | \psi_b \rangle|^2 = \left| \frac{1}{\sqrt{2}}(j\cos(\theta_b) + \sin(\theta_b)) \right|^2 = \frac{1}{2} \quad (9)$$

Looking at the coincidences,...

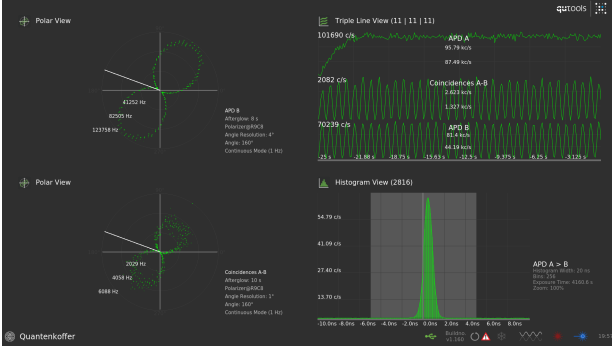


Fig. 10: Half Waveplate added, Source in $|H\rangle$, A in $|+\rangle$

We know that the wavefunction should be:

$$|\psi_f\rangle = \frac{1}{2}(j|H\rangle_a + |V\rangle_a)(j|H\rangle_b + |V\rangle_b) \quad (10)$$

This equates to:

$$\frac{1}{2}(-|HH\rangle + j|HV\rangle + j|VH\rangle + |VV\rangle) \quad (11)$$

Also noting our measurement state:

$$\begin{aligned} |\psi_{\text{target state selected by polarities}}\rangle &= |\theta_a \theta_b\rangle \\ &= \cos \theta_a \cos \theta_b |HH\rangle + \cos \theta_a \sin \theta_b |HV\rangle \\ &\quad + \sin \theta_a \cos \theta_b |VH\rangle + \sin \theta_a \sin \theta_b |VV\rangle \end{aligned} \quad (12)$$

We can get our expected probability of single-photon detection:

$$|\langle \theta_a \theta_b | \psi_f \rangle|^2 = \left| -\frac{1}{2} e^{j(\theta_a + \theta_b)} \right|^2 = \frac{1}{4} \quad (13)$$

Because our input is circularly polarized, as we vary the angle θ , we expect uniform intensity measurements, thus giving a polar plot similar to $r = \text{constant}$. However, this is not an entangled state since, after interacting with the quarter waveplate, the state becomes factorizable.

VI. DAY 3 APPROACH

In this laboratory exercise, we perform single-photon interference measurements. We utilized a beam splitter to form two beams, then used dielectric wedges to manipulate the group phase and phase velocity of each wave. These adjustments were used to make detections easier to view. The beams then go through a fiber coupled beamsplitter, forming an interference pattern that is detected by APD A and APD B.

VII. DAY 3 RESULTS AND ANALYSIS

From Figure 13, it appears that the coherence time τ_c is approximately $-7.5 - (-15.63) = 8.13[\text{ps}]$. We can use the formula $\Delta f \approx \frac{1}{\tau_c}$ to get $\Delta f \approx 123[\text{GHz}]$

Now, using the formula $\Delta\lambda = \frac{\lambda_0^2}{c} \Delta f$, we can find that $\Delta\lambda = 269[\mu\text{m}]$, implying that the wavelength range is from 809.731[nm] to 810.269[nm].

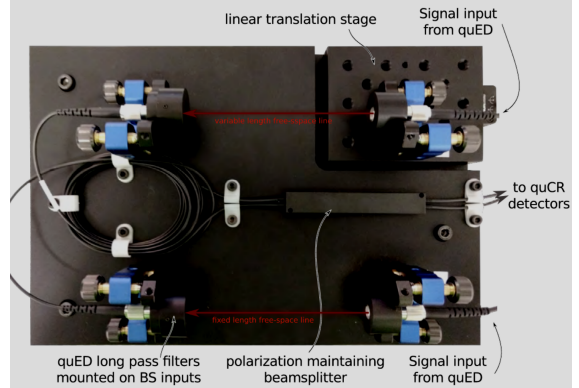


Fig. 11: Fiber Interferometer Setup

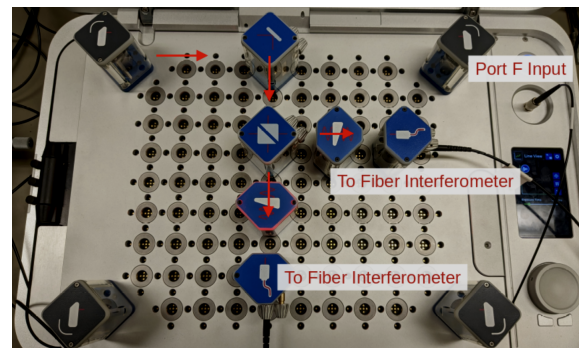


Fig. 12: Quantenkoffer Single-Photon Interference Optical Setup

Because of the interactions with the beam splitters, the detectors observe interference patterns that are π off phase. This makes sense from energy conservation, as a π off phase relation means that, when one interference pattern is at a maximum, the other is at a minimum. Thus, the input energy is still equivalent to the output energy.

My theoretical calculated value from the prelab is somewhat similar to my recently-calculated value. Factors that may be throwing my calculations off are small losses and misalignments are various points in my optical setup, thermal expansion of optical materials from body heat and other heat sources in laboratory, and minuscule table shifts that could potentially introduce unexpected nanometer-scale oscil-



Fig. 13: Quantenkoffer Measured Interference

lations. While many of these sources of error are tiny, the nanometer-scale measurements make a cumulation of these errors potentially-disastrous.

VIII. DAY 4 APPROACH

In this laboratory exercise, we investigate the Hong-Ou-Mandel (HOM) effect, where two single photons interfere at a beam splitter, leading to photon bunching at the output ports. This results in the formation of a highly entangled NOON state.

We set up beams that enter two wedges. The beams then go to the fiber setup. To observe the HOM effect, we manipulate the movement speed of the wedges and the position of one of the signal inputs on the fiber setup using a very precise linear transition stage. Minuscule changes affect the setup significantly, forcing changes in the wedge positions and linear transition stage to be extremely precise and intentional.

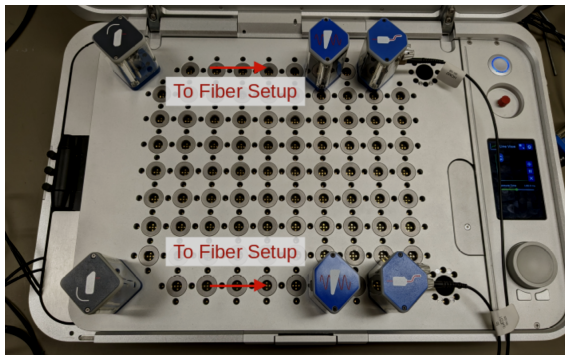


Fig. 14: Quantenkoffer HOM Optical Setup [6.2410 Github]

IX. DAY 4 RESULTS AND ANALYSIS

Figure 15 demonstrates the HOM dip detected. Using a timer, we found that the dip took approximately 9.375 seconds, which means the dip truly took $9.375[\text{ps}]$. Using $c = \frac{d}{t}$, $d = ct = (3 \cdot 10^8)(9.375 \cdot 10^{-12}) = 2.8[\text{mm}]$.

As a percentage of the total coincidences when not overlapped, the dip is approximately $\frac{50}{275} = 0.18$

Based on the previous histograms, I believe the coincidence timing is electronics-limited.



Fig. 15: HOM Dip

X. SUMMARY AND CONCLUSIONS

I will now address the post-lab questions:

Given the probability of coincidences is $P(\varphi) = \frac{\eta(1-V\cos(N\varphi))}{2}$, we can use the following provided formulas:

$$\Delta C_k^2 = kP(\varphi)(1-P(\varphi)) = \frac{k\eta}{2}(1-V\cos(N\varphi))(1-\frac{\eta}{2}+\frac{\eta}{2}V\cos(N\varphi)) \quad (14)$$

$$C_k(\varphi) = kP(\varphi) = \frac{k\eta}{2}(1-V\cos(N\varphi)) \quad (15)$$

$$\frac{dC_k(\varphi)}{d\varphi} \Big|_{\varphi_0} = \frac{kVN\eta}{2} \sin(N\varphi) \quad (16)$$

$$\delta p = \frac{\Delta C_k^2}{(\frac{dC_k}{d\varphi} \Big|_{\varphi_0})^2} = \frac{k\eta}{2} \frac{(1-V\cos(N\varphi))(1-\frac{\eta}{2}+\frac{V\eta}{2}\cos(N\varphi))}{(\frac{KVN\eta}{2} \sin(N\varphi))^2} \quad (17)$$

Based on my derived formula, $-1 < V < 1$ should guarantee extreme sensitivity.

As observed in lab, producing a NOON state is extremely sensitive and difficult to set up and examine. Small setup issues mentioned before, such as small energy losses throughout the system, small vibrations in the area, and unaccounted heat sources causing length fluctuations. To overcome these barriers, high-quality materials would be needed to mitigate losses, as well as a method to reduce vibrations (i.e. floating a table) and a method to reduce heat fluctuations (i.e. a controlled heat environment).

In general, we were able to determine quantum entanglement states and outcomes, learn essential calibration methods of optical setups, and generate sensitive NOON states.

The extreme sensitivity to slight changes in optical setups as observed in this laboratory experience set the foundations for modern and future ultra-sensitive sensors. Entanglement also promises rapid enhancements in communication speeds and fool-proof cryptography.